Automatic segmentation and measurement of axons in microscopic images.

O. Cuisenaire[1], E. Romero[2], C. Veraart[2] and B. Macq[*1]

[1] Communication and Remote Sensing Laboratory, Université catholique de Louvain, B-1348 Louvain-la-Neuve, Belgium.
[2] Neural Rehabilitation Engineering Laboratory, Université catholique de Louvain, B-1200 Brussels, Belgium.

ABSTRACT

We propose a method for the automatic segmentation, recognition and measurement of neuronal fibers in microscopic images of nerves. This permits a quantitative analysis of the distribution of the areas of the fibers, while nowadays such morphometrical methods are limited by the practical impossibility to process large amounts of fibers in histological routine. First, the image is thresholded to provide a coarse classification between myelin (black) and non-myelin (white) pixels. The resulting binary image is simplified using connected morphological operators. These operators simplify the zonal graph, whose vertices are the connected areas of the binary image. An appropriate set of semantic rules allow us to identify a number of white areas as axon candidates, some of which are isolated, some of which are connected. To separate connected fibers – candidates sharing the same neighboring black area - we evaluate the thickness of the myelin ring around each candidate area through Euclidean distance transformation by propagation with a stopping criterion on the pixels in the propagation front. Finally, properties of each detected fibers are computed and false alarms are suppressed. The computational cost of the method is evaluated and the robustness of the method is assessed by comparison to the manual procedure. We conclude that the method is fast and accurate for our purpose.

Keywords: Histology, Fibers counting, Segmentation, Recognition, Mathematical morphology, Distance transformation, Connected operators, Zonal graph.

1. INTRODUCTION

The central nervous system of humans or animals consists of billions of nerve cells called neurons. These neurons are connected to each other through axons. Information between neurons is transmitted in the form of action potentials propagating along the axons. Neurons within the central system may be connected to sensory organs or to muscle fibers. In that case, axons are generally surrounded by a myelin sheet, and are then called neuronal fibers. Bundles of neuronal fibers are generally arranged in between parts of the central nervous system and sensory or motor organs. They form the peripheral nerves.

Since more than a century ago, morphometrical analysis is a well-know technique, widely and routinely used in studies of the peripheral nerves [1]. The fiber size distribution is used to diagnose nerve degeneration in both research [5] and clinical [3] applications.

Because there are thousands of fibers in a nerve, manual procedures to count and measure fibers are always highly time consuming, and often impractical. Besides, manual procedures always rely on sampling, i.e. on the choice of a reduced set of images among those available in a cut of the nerve. As pointed out in [7], there is no simple adequate sampling scheme for estimating the myelinated fiber size distribution in peripheral nerves, because of the heterogeneous nature of this distribution. Therefore, manual procedures will not only be impractical, but also unreliable.

Cell counting algorithms are usually divided in two parts. First, the image is analyzed with a local operator, which provides a classification of the pixels into classes defined by the various tissues one expects to find in the image. For this stage, most algorithms rely on thresholding, sometimes preceded by filtering [4,6,12]. Secondly, the image is analyzed at the structural level using a variety of tools such as region growing segmentation [4], grouping of edge elements [6], or mathematical

[*] Correspondance: Email: Macq@tele.ucl.ucl.ac.be; WWW: http://www.tele.ucl.ac.be/PEOPLE/bm.html

morphology [12]. Unfortunately, none of these method can handle multi-part objects such as axons surrounded by a myelin sheet.

Lately, many authors have relied on active contour models, or snakes [8,11,13], to handle both local and structural analysis in one step. After detecting candidates through a global tool such as the Hough transform, each cell is processed individually with an explicit active contour model evolving towards the real contours of the cell. Unfortunately, such method may be too computationally complex for the large data sets required by a full histological study.

Furthermore, it is unclear how any of the above models could handle the large size variability encountered in the fibers found in peripheral nerves.

In this paper, we propose a new automatic method for the recognition of neuronal fibers, based on the connected morphological operators to identify candidate areas, and on the Euclidean distance transformation to separate aggregate fibers. In section 2, we describe the data, i.e. how the images were acquired and how axons can be recognized in these images. Section 3 presents the algorithm in four steps, binarization, filtering with connected morphological operators, separation of adjacent fibers and false alarm detection. In section 4, we present experimental results on a large set of images. Those results are discussed in section 5.

2. MATERIAL TO BE PROCESSED

2.1. Image acquisition

A cat sciatic nerve was fixed with a Paraformaldehyde 4%, Dextran 3,5% and PBS solution. A 0.5 cm fragment of the nerve was conserved in Karnosky's fixative for 24 hours, then postfixed in 1% Osmium tetroxyde. 1 µm thick sections were cut on a Reichter ultracut microtone (Reichter, Wien, Austria) and stained with toluidine blue. Afterwards, transparences were obtained from a Zeiss microscope at high magnification and digitized at a 1850 x 1234 pixels size, with a acquisition system Nykon 25-1000. A microscale (0.01 mm, Wild, Switzerland) was also digitized with the same system for scaling. The pixel size was found to be 0.1135 µm. Typical images are shown at Figure 1.

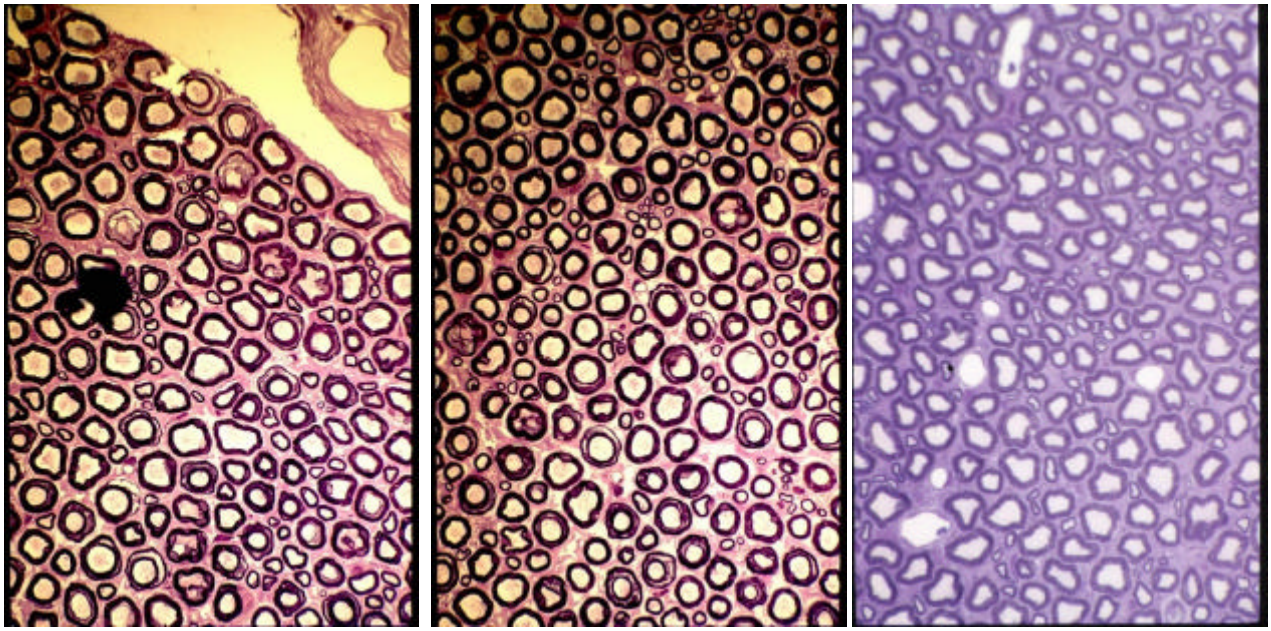

Figure 1: typical 1850x1234 pixels images under study. Left and center image are from the same nerve and were acquired under similar conditions. Right image comes from another nerve.

2.2. Morphological features of axons

After this process, myelin appears darker in the images. This provides us with a way to recognize neuronal fibers as objects that share the following features:

- A clear region surrounded by a dark myelin sheet with a constant width.
- A rather circular shape.
- A ration d/D close to 0.6, with d the diameter of the axon, and D the diameter of the whole fiber [2].

Unfortunately, axons also present a number of highly variable features that may hinder the efficiency of detection algorithms. For instance,

- For mixed nerves containing both sensitive and fiber axons – such as the sciatic nerve - the diameter of fibers can vary between 2 and 20µm.
- Axons can be isolated or densely packed together.
- Fixation and coloration problems can lead to brighter spots in the myelin rings, multiple rings, etc.

Those problems are illustrated at Figure 2.

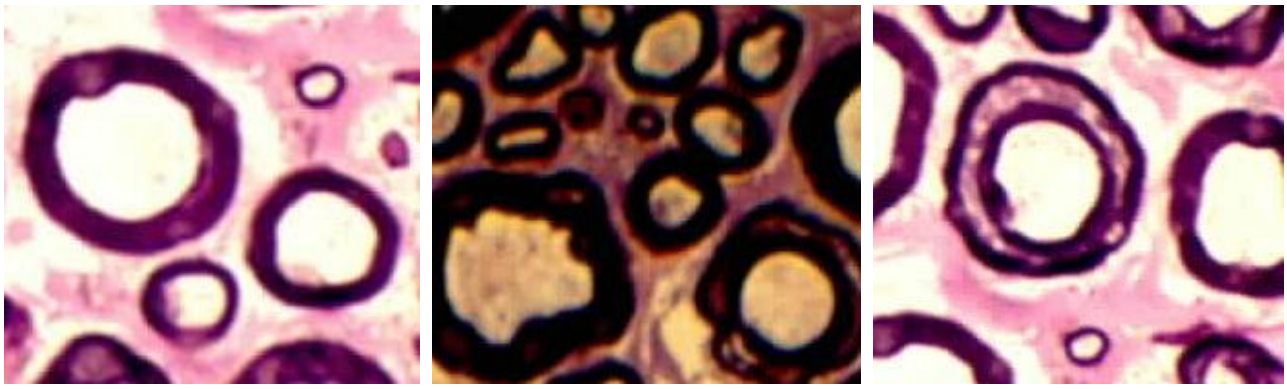

Figure 2 : Zooms on the central image of Figure 1 illustrate irregularities in fibers to be detected. Left: size can vary from 2 to 20 µm (diameters). Center: densely packed axons are connected. Right: bad fixation and coloration leaves bright rings in the myelin.

3. ALGORITHM

The processing is divided in four parts. First, pixels are classified as myelin (black) or non-myelin (white) pixels according to their luminance level. Secondly, the resulting binary image is simplified using connected morphological operators according to rules derived from the description of axons made in the previous section. At this stage, axon candidates are identified as leaves of the zonal graph. Thirdly, adjacent axons are separated using a distance criterion. Finally, strict criteria are checked for each axon candidate to avoid false detection.

3.1. Pixel classification

First, pixels of the image are classified as belonging to the myelin sheets or not. After the fixation and coloring process (see section 2.1), myelin appears darker than the endoneurium and the inside of the axons. Therefore, classification can be obtained by a simple threshold.

The choice of the threshold level can be made from a simple heuristic analysis of the histogram of the gray levels in the image. The typical luminance of myelin pixels is evaluated as the luminance for which 15% of pixels are darker. We chose the level of the threshold at a fixed constant above that luminance, typically 20 for values coded between 0 and 255.

As pointed out in [10], locally adaptive thresholds are more robust than global ones. In our case, this is particularly needed since the image acquisition often leads to inhomogeneous illumination. Therefore, the histogram analysis is performed

locally on areas including a few axons, typically squares of 25 x 25 µm. In order to keep the computational cost low, this analysis is only performed on a few locations and the threshold levels are bi-linearly interpolated in between.

Typical results are shown at Figure 3. These results are quite insensitive to the choice of the two parameters above within reasonable bounds. In practice, parameters are manually chosen by the operator on one image per nerve, and applied to the set of all images from the same nerve (there are typically 100 images per nerve).

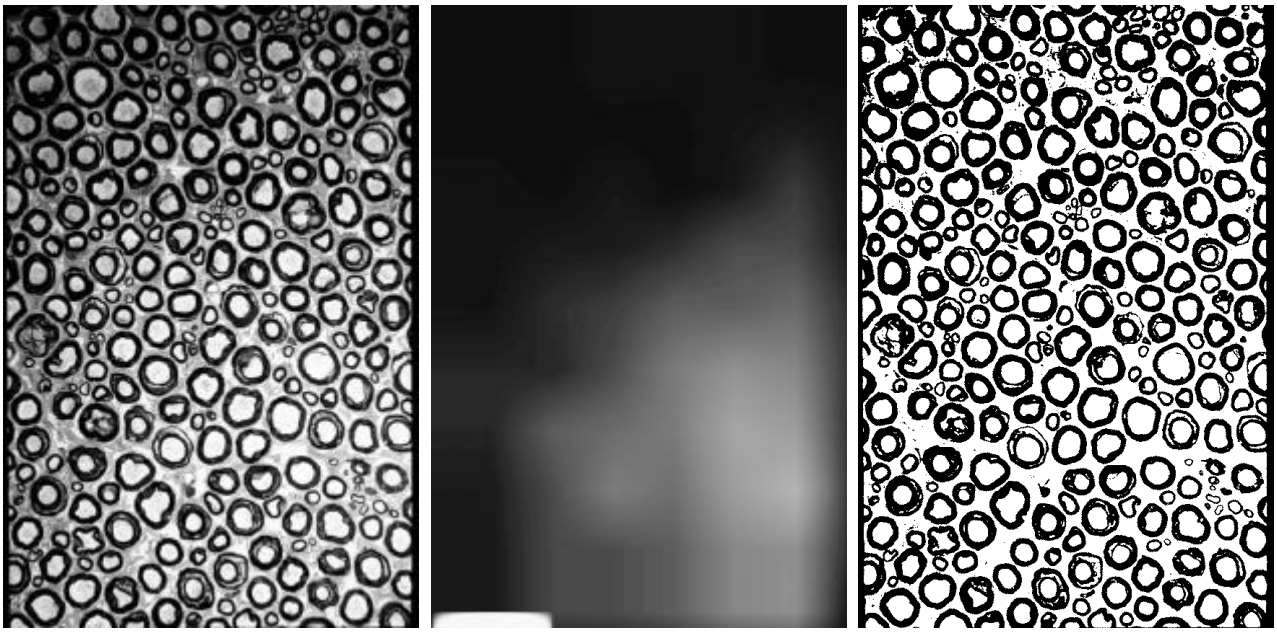

Figure 3: from left to right: original image, local threshold levels (with an increased contrast), resulting binary image.

3.2. Connected operators filtering

The resulting binary image has a number of artifacts (see section 2.2) which can best be expressed in terms of regions and their properties. Heijmans [14] proposes a formalism, connected morphological operators, which allows us to process the image in the same terms.

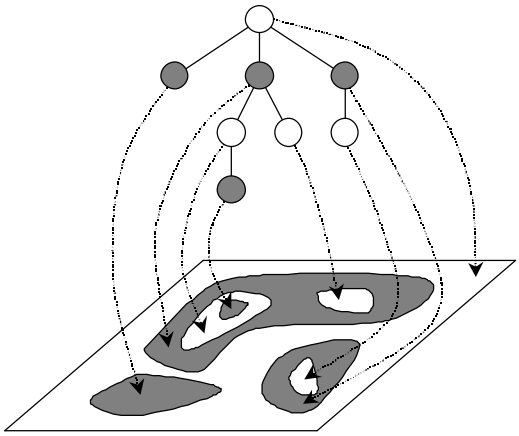

Figure 4 : Zonal graph (top) associated with the binary image (bottom)

As illustrated at Figure 4, the binary image is considered as a partition P(X) of the set X of pixels into black and white regions. The *zonal graph* of the image is the graph that takes the regions of P(X) as vertices and whose edges are represent

the adjacency of the regions corresponding to the two linked vertices. Furthermore, the representation specifies for each vertex whether it belongs to the foreground or the background. A morphological operator y is called connected if the resulting partition $P(y(X))$ is coarser than $P(X)$, for any set X, which means no new edges are introduced and connected zones are left untouched or changed altogether. In the common case where the connectivity is based on adjacency, connected operators can more easily be described and implemented in terms of recoloring and merging of the corresponding zonal graph (Figure 5).

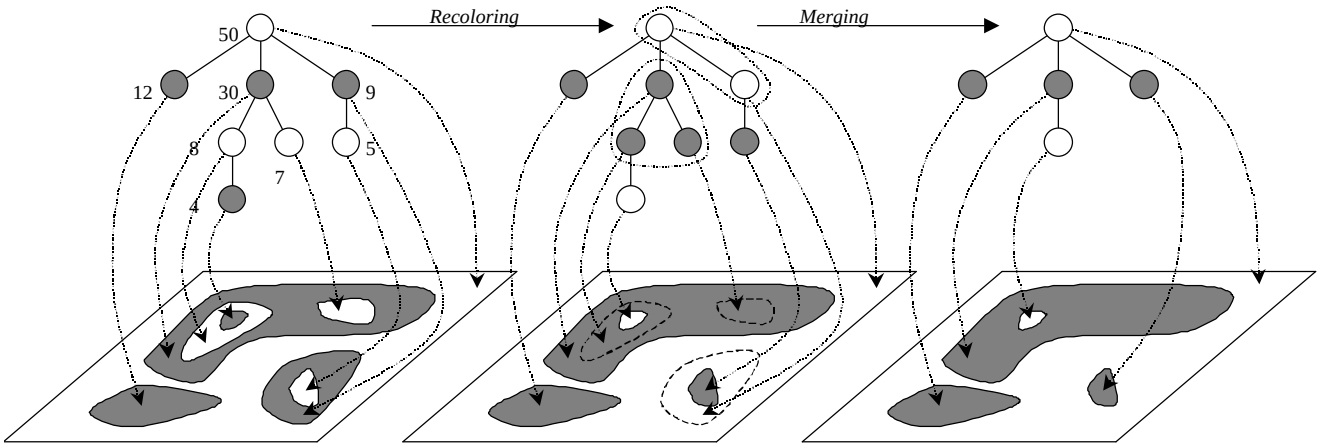

Figure 5 : the area operator flips zones with an area of less than 10 (see numbers printed on the left figure). It can be seen as a recoloring and merging of vertices in the zonal graph.

The best know connected morphological operator is the opening by reconstruction, where objects too small to contain the structural element of the original erosion are deleted and objects large enough are left unchanged. More complex criteria can of course be defined, either considering each zone separately – it is then called a grain operator – or considering the relationships between zones and their neighbors. In what follows, we will use both.

In our case, we use the 8-adjancency for foreground pixels and 4-adjacency for background pixels. This defines a topology that is similar to the continuous case, and in particular the zonal graph is then a tree, i.e. a graph without cycles. A number of connected operators are then applied successively in order to remove the artifacts described at section 2.2 and to identify axon candidates.

- Noise in the original image may lead to small mislabeled areas in the binary image. Those are removed by applying the area operator (Figure 5), that is the operator that switches the color of all zones whose area are smaller than a given value. As such, the area operator is not stable. Instead, we chose to restrict its action to the leaves of the zonal tree, i.e. the regions with only one neighbor. We apply this "leave area operator" until we reach idempotence. The value for which areas are recolored is chosen smaller than the smallest axons, for instance 0.5 µm² or 40 pixels.
- Axons always have a bright center surrounded by a black ring. Therefore black leaves in the zonal tree cannot represent a useful feature and can be removed. We apply the "black leave operator" once.
- Fixation problems can separate the myelin sheet in two parts, as illustrated at Figure 2c. In the binary image, this appears as a white ring surrounded by two black rings. These rings can easily be detected by compu.ting the gravity center of all white areas. The centers of rings are not included inside the area itself. Two cases can appear: either the ring is open and the ring is a leaf of the zonal graph. It is then merged with its only neighbor. Or the ring is closed and has 2 neighbors in the zonal graph. The three vertices of the graph are then merged together as a black area, i.e. the ring is recolored in black.

Finally, *axon candidates* are identified as white leaves in the zonal tree satisfying both a size criterion ($1\ \mu m < d < 12\ \mu m$) and a shape criterion ensuring the compactness and approximate circularity of the center of the axon, typically the ratio between square of the perimeter of the zone and its area is kept below a certain level.

3.3. Separation of connected fibers

Unless the axons are very sparse in the image considered, some of them will be connected in the resulting image. In the zonal tree, it means that several white leaves that are axon candidates share the same black vertex neighbor. This section deals with the division of the corresponding black zone into sub-regions that are either myelin sheets surrounding axon candidates or artifacts to be merged with the background. Let us consider the example of the black area in Figure 6 and the corresponding zonal graph of Figure 7. Among the 9 leaves of the graph, leaves "x" and "y" have been discarded at the previous stage, because they lack circularity to be proper axon candidates. Among the 7 remaining candidates, areas 1 to 6 are true axons while area 7 is an artifact. In the black area itself, some pixels are indeed myelin while others are artifacts.

Let us first consider a single white area. We evaluate the thickness of the myelin sheet around it as follows: we define X_d the set of pixels at distance d of a set X of pixels as

$$X_d = (X \oplus S_{d+1}) \cap (X \oplus S_d)^c$$

with S_d a circular structural element of size d and $\oplus$ the Minkowski addition. Then, we define the typical thickness of the myelin sheet around a white area X as the smallest distance d for which there are more white than black pixels in X_d.

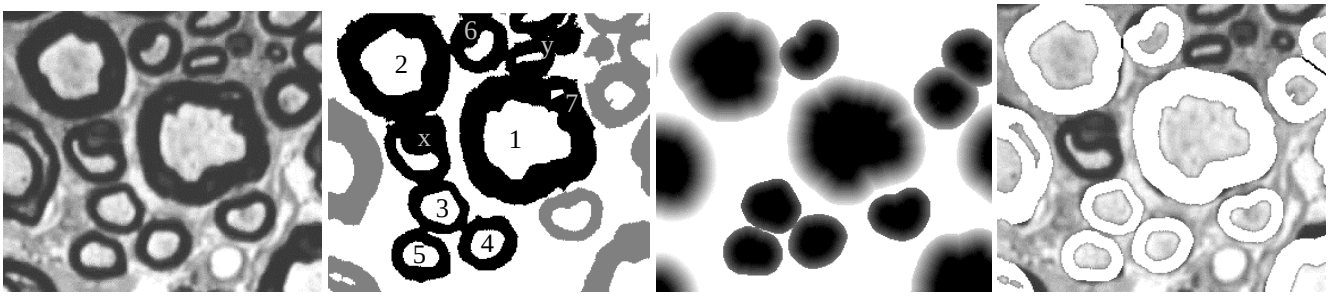

Figure 6: Axon separation by distance transform. From left to right: original image; result of the connected operators filtering (the black area is one connected area that needs to be split into several axons); distance map; axons found overlaid on the image.

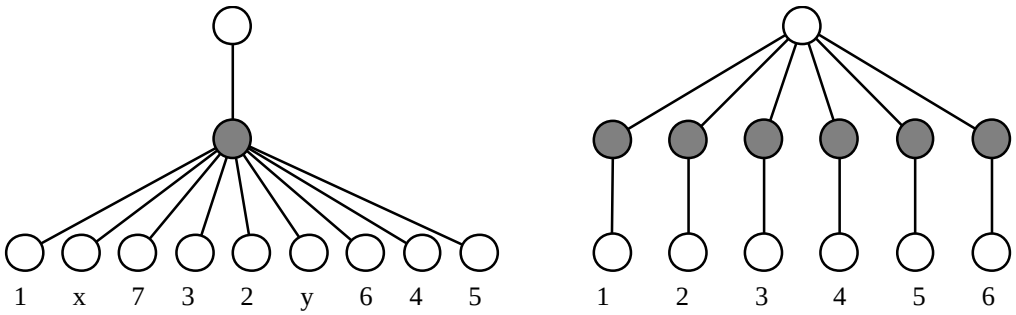

Figure 7: zonal graphs of the region of interest before and after axon separation.

This can be very efficiently implemented using the approximate Euclidean distance transformation (EDT) by propagation defined in [9] or the exact EDT defined in [15]. These algorithms compute distance maps, i.e. images where the value of each pixel is the Euclidean distance from this pixel to a set of pixels X, that is the shortest distance from that pixel to a pixel of the set X. Initially, the map is set to 0 for pixels of X and to the maximum integer for all others, and the pixels of X are stored in a dynamic queue. Then, for each pixel of the queue, we consider that the nearest pixel of X is the also the nearest pixel of X for its neighbors. If this leads to a smaller distance value than currently in the map, this value is updated and the neighbor is inserted in the queue. In order to reduce computational cost, the pixels in the queue must be treated in the order of increasing distance value rather than in a simple FIFO order. This is done by replacing the single queue by a number of buckets corresponding to each possible distance value, or rather to the square of each possible value, so that only integers are considered. Buckets are then emptied in order of increasing distance values.

With this algorithm, the set X_d of pixels at distance d of X is the set of all pixels present in the buckets after bucket d has been processed. The amount of black and white pixels in X_d is dynamically computed for every distance d and the propagation process stopped as soon as the termination condition is reached. The pixels that were reached by the propagation process – and only those - will be considered as belonging to the myelin sheet around our axon candidate.

Let us now consider all the "axon candidates" areas that are leaves of the same black area in the zonal graph. We apply the above procedure to each candidate, in decreasing order of size. In our example of Figure 6, this efficiently separates fibers numbered 1 to 5. For area number 6, the propagation process reaches pixels that were previously considered as belonging to the myelin sheet around area number 2. These pixels are relabeled if needed. The resulting edge between the two fibers corresponds either to the thickness of the smallest fiber, or to the iso-distance between the two white areas.

For area number 7, we realize that it is included inside the previously computed myelin sheet around area 1. This additional test, done before each distance propagation, shows if an area is not a true fiber, but rather an artifact to be discarded.

3.4. False alarm detection

Obviously, the automated detection of axons can lead to two types of errors: misdetection when a true fiber is not found and false alarm when an image feature is wrongly considered to be a fiber. False detection is considered a worse problem since it is most likely to introduce a bias in the fiber distribution statistics, as most false alarms lead to objects of small size, which would bias the computed fiber size distribution. Misdetection is only detrimental if the misdetection rate is size dependant, which does not appear to be the case.

In order to minimize the number false alarms, we rely both on a intrinsic confidence measure for each detected fiber and on a conflict measure that uses information from the surrounding features. The confidence measure relies mostly on the d/D ratio between the diameter d of the inner white region and the diameter D of the complete fiber. This ratio should be reasonably close to 0.6.

For densely packed fibers, we observe that false alarms often occur in the space between 3 neighboring axons. These can easily be detected by looking at the pixels on their edges. Most of those pixels belong to other axons, while it belongs to the the background of the image for true axons. Also, for images including the edge of the nerve, such as Figure 1a, some external features can be mistaken for fibers. Those too can easily be detected since they are isolated from the rest of the detected fibers. The combination of the edge and isolation criteria give the conflict measure.

4. EXPERIMENTAL RESULTS

In order to assess the accuracy of our method, we have measured the false alarm and misdetection rates on a set of 30 images including a total of more than 5000 fibers, i.e. on half the images for one fascicle of a nerve. The detected fibers are superimposed on the original image as illustrated at Figure 8. For each image, false alarms and missed fibers are counted by an expert in the field. The number of detected entities is computed by the program itself, and the true number of fibers is computed from those three values.

The results of this test are shown at Table 1. The average false alarm rate is 2.5 % and the misdetection rate is 11%. This is perfectly reasonable given the later use of this data, which is to compute and compare the histograms of fiber size distribution in various nerves. In any case, it is better than what can be expected from a manual procedure which would rely on the sampling of the set of available images.

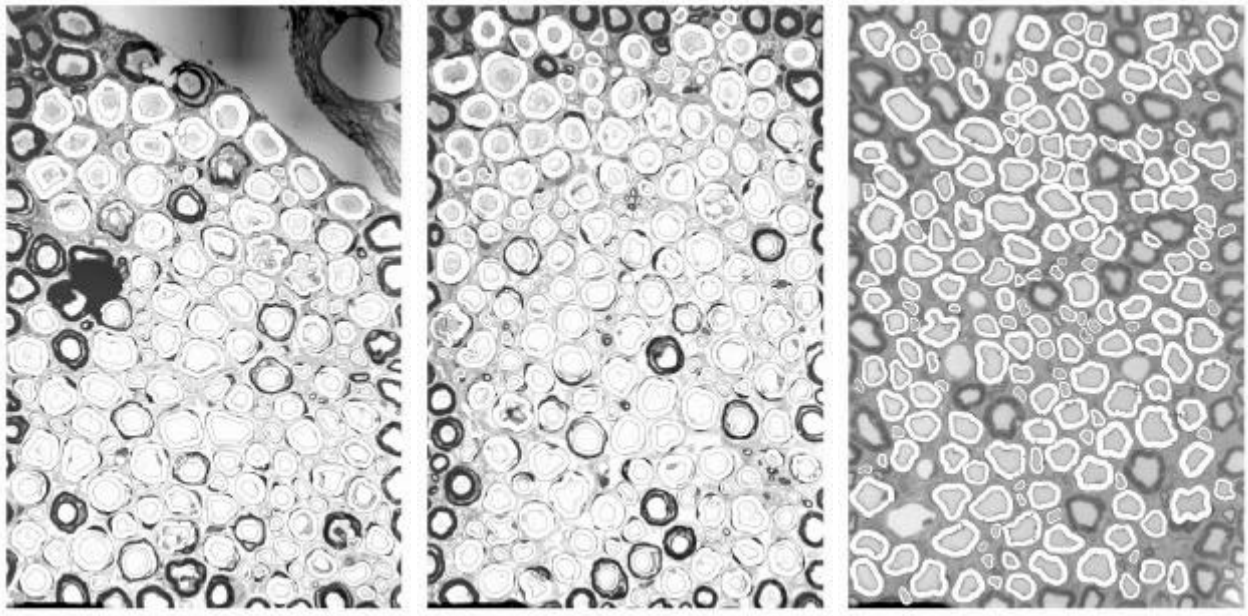

Figure 8 : Detected fibers overlaid upon the original images of Figure 1.

Image ID	# of fibers	# found	# of fibers missed	# of false alarms
1	75	59	16	0
2	143	127	18	2
3	223	181	43	1
4	128	122	9	3
5	171	166	8	3
6	185	173	18	6
7	186	162	26	2
8	194	186	15	7
9	135	126	12	3
10 Fig. 8a	178	154	30	6
11 Fig. 8b	230	210	25	5
12	212	181	36	5
13	188	162	28	2
14	189	172	23	6
15	83	69	16	2

Image ID	# of fibers	# found	# of fibers missed	# of false alarms
16	197	172	31	6
17	195	175	25	5
18	214	196	23	5
19	249	232	26	9
20	247	224	25	2
21	98	95	7	4
22	229	202	36	9
23	233	202	36	5
24	229	206	27	4
25	200	183	21	4
26	204	189	23	8
27	178	165	17	4
28	203	178	29	4
29	190	179	17	6
30	210	187	25	2
TOTAL	5596	5035	691	130

Table 1: Detection results for the set of 30 test images.

5. DISCUSSION

The method we have developed is fully automatic when the various parameters have been set to appropriate values. These values are constant for a given fixation, coloration and acquisition procedure. In practice, the operator selects the appropriate parameters for one image and applies them to all images from the same nerve.

The easiest way to improve the results is to introduce some further level of interactivity in the process, especially as a post-processing of the results. Obviously, the false alarm rate can be brought down to zero with an operator pointing at those errors in the overlaid images of Figure 8. The misdetection ratio could also be lowered by pointing to the misdetected fibers and forcing the corresponding leaves in the zonal graph to be axon candidates and to be considered first in the fiber

separation process. Because it only concerns a few fibers per image – typically 2.5% of all fibers - this level of interactivity does not represent too much of a burden for the operator.

As pointed out earlier, the computational cost is a critical parameter, especially if one wants to introduce interactivity in the process. Besides, in order to be statistically relevant, an histological study requires the processing of hundreds of images such as those of Figure 1, which represents several hundreds of Megabytes of data for each nerve in the study, and thousands of fibers to be detected. In our method, most of the processing is done on the zonal graph instead of the image. Because the zonal graph is orders of magnitude smaller than the image, the corresponding processing time is negligible. The most costly stages of the process are then the thresholding, the creation of the zonal graph and the separation of the axons by distance transformation. The creation of the graph requires the labeling of the image and the linking of neighboring areas, for which a couple of raster scans are needed. The computation of dilations by Euclidean distance transformation as in [15,9] requires one or two passes over each pixel in the propagation area. In total, the whole processing has a complexity linearly proportional to the number of pixels in the image. On a SUN sparc ultra 1 workstation, the processing time for each image is approximately one minute, and the processing time for a complete nerve varies between one and two hours.

6. CONCLUSION

We have elaborated a method to detect neuronal fibers in microscopic images. Because those fibers are defined from two objects – a white center surrounded by a black ring – the zonal graph and connected morphological operators defined upon it are appropriate tools to isolate good axon candidates. The evaluation of the myelin sheet thickness and the separation of aggregate fibers is performed using distance propagation until a criterion on the propagation front is met. The experimental results show a good accuracy of the method, at a reasonable computational cost.

ACKNOWLEDGMENTS

Olivier Cuisenaire's work is funded by the Belgian FRIA fund (Fonds pour la Formation à la Recherche dans l'Industrie et dans l'Agriculture). Eduardo Romero's work is partially supported by grant # BMH4-CT-96-0897 (Project *Sensations*), BIOMED program of the EU Commission. We wish to thank J.F. Denef and J. Delbeke for their help in collecting the data for this study.

Figures 4 and 5 are adapted from originals found in [14].

REFERENCES

1. C.S. Sherrington, "On the anatomical constitution of nerves to skeletal muscles; with remarks on recurrent fibers in the ventral spinal nerve-root", *J. Physiology* **17**, pp. 211-258, 1894.
2. W.A.H. Rushton, "A theory of the effects of fiber size in medullated nerve.", *J. Physiology* **115**, pp. 101-122, 1951.
3. F. Buchtnal and F. Behse, "Sensory action potentials and biopsy of the sural nerve in neuropathy", *Proc. of the Int. Symp. on Peripheral Neuropathies*, Milan, June 26-28, 1978.
4. A.K. Jain, S.P. Smith and E. Backer, "Segmentation of muscle cell pictures: a preliminary study.", *IEEE Trans. on Pattern Analysis and Machine Intelligence* **2**, pp. 232-242, 1980.
5. P.J. Dyck, J. Karnes, P. O'Brien, H. Nukada, A Lais and P Low, "Spatial pattern of nerve fiber abnormality indicative of pathologic mechanism", *Am. J. of Pathology* **117**, pp. 225-238, 1984.
6. C. Garbay, "Image structure representation and processing: a discussion of some segmentation methods in cytology.", *IEEE Trans. on Pattern Analysis and Machine Intelligence* **8**, pp. 140-146, 1986.
7. S. Torch, P. Stoebner, Y. Usson, G. Drouet D'Aubigny and R. Saxod, "There is no simple adequate sampling scheme for estimating the myelinated fiber size distribution in human peripheral nerve: a statistical ultrastructural study.", *J. Neuroscience Methods* **27**, pp. 149-164, 1989.
8. A. A. Amini, T.E. Weymouth and R.C. Jain, "Using dynamic programming for solving variational problems in vision", *IEEE Trans. On Pattern Analysis and Machine Intelligence* **12** (9), pp. 855-867, 1990.
9. I. Ragnelmam, "Fast erosion and dilation by contour processing and thresholding of distance maps." *Pattern Recognition Letters* **13**, pp. 399-409, 1992.
10. O.D. Trier and T. Taxt, "Evaluation of binarization methods for document images.", *IEEE Trans. on Pattern Analysis and Machine Intelligence* **17**, pp. 312-315, 1995.

11. Y-L. Fok, J.C.K. Chan and R.T. Chin, “Automated analysis of nerve-cell images using active contour models.”, *IEEE Trans. on Medical Imaging* **15**, pp. 353-368, 1996.
12. J.-Ph. Thiran and B. Macq, “Morphological feature extraction for the classification of digital images of cancerous tissues.”, *IEEE Trans. on Biomedical Engineering* **43**, pp. 1011-1019, 1996.
13. A. Elmoataz, S.Schüpp, R. Clouard, P. Herlin and D. Bloyet, “Using active contours and mathematical morphology tools for quantification of immunohistochemichal images”, *Signal Processing* **71**, pp. 215-226, 1998.
14. H.J.A.M. Heijmans, “Connected morphological operators for binary images”, *Computer Vision and Image Understanding* **73** (1), pp. 99-120, 1999.
15. O. Cuisenaire and B. Macq, “Fast Euclidean morphological operators using local distance transformation by propagation.”, *7th Int. Conf. on Image Processing and its Applications*, Manchester, July 12-15, 1999.